



Graphene Oxide Incorporated Forward Osmosis Membranes With Enhanced Desalination Performance and Chlorine Resistance

Zhanguo Li¹, Yi Wang^{1,2*}, Mengwei Han¹, Dayong Wang³, Shitong Han¹, Zequn Liu⁴, Ningyu Zhou^{4*}, Ran Shang¹ and Chaoxin Xie⁴

¹ State Key Lab of NBC Protect for Civilian, Beijing, China, ² Water Industry and Environment Engineering Technology Research Centre, Chongqing, China, ³ Service Bureau of Agency for Offices Administration of the CMC, Beijing, China, ⁴ Department of Military Facilities, Army Logistics University, Chongqing, China

In this work, grapheme oxide (GO) nano-sheets were synthesized and dispersed in the aqueous phase for the interfacial polymerization (IP) process to develop a new type of thin-film composite (TFC) membranes for forward osmosis (FO) applications. The effects of the GO concentrations on the membrane surfaces and cross-sectional morphologies and FO desalination performances of the as-prepared TFC membranes were investigated systematically. Compared with the control membrane, the optimal GO-incorporated TFC membrane displayed higher water flux, less specific reverse solute flux (SRSF) and lower structure parameter. Moreover, the optimized membrane showed 75.0 times higher chlorine resistance than the control membrane. In general, these new type of membranes could be an effective strategy to fabricate high-performance FO membranes with good desalination performance and chlorine resistance.

Keywords: forward osmosis, GO nano-sheets, thin-film composite membrane, desalination performance, chlorine resistance

INTRODUCTION

Desalination refers to the process of removing salts or minerals dissolved in seawater or brackish water to obtain water for human and animal consumption, irrigation and industrial process, which is a significant technology can effectively alleviate the lack of fresh water for the whole global (Marcovecchio et al., 2005). Common desalination methods include thermal methods represented by multi-stage flashing and multi-effect evaporation and membrane-based techniques represented by electro-dialysis, nano-filtration (NF) and reverse osmosis (RO) (Darwish and ElDessouky, 1996; Khawaji et al., 2008). Among them, RO technology is currently the most popular technology and more than 50% of the world's 15,000 desalination plants are RO-technology-based (Greenlee et al., 2009).

Despite the wide application of RO, this technology has some disadvantages such high energy consumption, low water recovery and severe brine pollution. Forward osmosis (FO) technology has been widely concerned by researchers and industrial circles recently. This technology utilizes the difference of osmotic pressure (or chemical potential) between a low-concentration feed solution (FS) and a high-concentration draw solution (DS) to drive water molecules across a semi-permeable membranes (Zhao et al., 2012). Compared with RO, the FO technology has shown advantages, such as low energy input of operation (Mazlan et al., 2016), efficient rejection of contaminants

OPEN ACCESS

Edited by:

Liguo Shen,
Zhejiang Normal University, China

Reviewed by:

Peng Lu,
Ningbo University, China
Xiu Wen Cheng,
Lanzhou University, China

*Correspondence:

Yi Wang
wangyi102205@sina.com
Ningyu Zhou
zningyu69@163.com

Specialty section:

This article was submitted to
Green and Sustainable Chemistry,
a section of the journal
Frontiers in Chemistry

Received: 06 November 2019

Accepted: 05 December 2019

Published: 10 January 2020

Citation:

Li Z, Wang Y, Han M, Wang D, Han S,
Liu Z, Zhou N, Shang R and Xie C
(2020) Graphene Oxide Incorporated
Forward Osmosis Membranes With
Enhanced Desalination Performance
and Chlorine Resistance.
Front. Chem. 7:877.
doi: 10.3389/fchem.2019.00877

(She et al., 2013; Kong et al., 2014), and less propensity of membrane fouling (Emadzadeh et al., 2014a; Salehi et al., 2017). More recently, polyamide thin film composite (PA-TFC) membranes have been widely studied due to their high mechanical strength, satisfactory salt rejection and hydrolytic stability (Sukitpaneemit and Chung, 2012; Han et al., 2016).

Although PA-TFC membranes possess many advantages, its resistance to disinfectants with chlorine needs to be further improved for FO's wide practical applications. This is because the pervasive biological fouling is the major cause decreases membrane performance (Mi and Elimelech, 2010; Xue et al., 2016). Thus, disinfectants with chlorine for controlling bio-fouling or cleaning agents are needed in water treatment process, which can result in changes of the polyamide chains by the N-chlorination, Orton rearrangement, and directing chlorination reactions (Verbeke et al., 2017), consequently cause the sharp decline in membrane salt rejection. Apart from this, conventional PA-TFC membranes also face the problem of low water fluxes ascribed to their relatively hydrophobic and thick surfaces (Emadzadeh et al., 2013; Ma et al., 2017). The water molecules need to pass through the PA layer, thus its thick thickness and hydrophobicity make water transfer lower due to the increased membrane mass transfer resistance. It has been proved that the thinner and more hydrophilic PA layer improves the membrane water permeability of the PA-TFC membrane (Han et al., 2012; Wang et al., 2016). Based on the above two issues, PA-TFC membranes with improved chlorine resistance and thin active layer are highly demanded.

Many efforts have been devoted to improve these performances of FO PA-TFC membranes. Recently, various nano-materials have been widely studied to be incorporated into the PA layer to enhance the TFC membranes performances and showed great performance improvements, such as nano-silver, nano-titanium dioxide, nano-silica and hydroxide nanoparticle, etc. (Emadzadeh et al., 2014b; Niksefat et al., 2014; Liu and Hu, 2016; Lu et al., 2016, 2018). Among them, graphene oxide (GO), a promising two-dimensional carbon nano-material, has attracted great attention in the material research field. Its excellent physical properties coupled with flexibility in chemical functionalization ascribed to the abundant oxygen-containing functional groups, make GO an excellent candidate for various applications (Hu and Mi, 2013). Mariana Ionita et al. added GO in the preparation of ultrafiltration polysulfone (PSf) membrane to increase the water flux of the membrane. At the same time, the thermal stabilities and mechanical properties of these GO-incorporated PSf membranes were also significantly improved, but the required GO concentration was as high as 1.0 wt% (Ionita et al., 2015). Ho Kyong Shon's group studied similar PSf-GO based substrate for interfacial polymerization to form the PA layer of TFC FO membranes. Results revealed that at a relatively low amount of GO addition (0.25 wt%), the as-prepared membranes showed not only significantly improved water permeability but also effective PA layer formation (Park et al., 2015). In addition, Hee-Ro Chae et al. added only 76 ppm GO to the aqueous phase of the interfacial polymerization (IP) process to prepare RO membranes, these membranes possessed

improved water flux, salt rejection as well as anti-fouling properties (Ali et al., 2016).

Inspired by these outstanding work, in this paper, we first applied low-concentration GO nano-sheets in IP process for FO membranes fabrication. Mainly based on the following three reasons: Firstly, due to the two-dimensional capillary effect of GO nano-sheets, the water flux of the GO-incorporated FO membrane can be improved while remaining the salt rejection performance (Ali et al., 2016); Secondly, the abundant hydrophilic functional groups in the GO nano-sheets would increase the membrane water flux and thus desalination performance; Finally, the PA active layer would be protected by GO nano-sheets thus improved its chlorine resistance. The FO membranes were synthesized by adding different concentrations of GO nano-sheets into the aqueous phase of IP process. A series of characterizations were conducted to understand the influence of GO nano-sheets on the active layer morphology and hydrophilicity. FO membrane experiments were performed to evaluate the desalination performance and chlorine resistance as well as determine the most suitable GO nano-sheets incorporation concentration.

EXPERIMENTAL

Materials

PSf with 22,000 Da average molecular weight (Sigma-Aldrich, USA), polyvinylpyrrolidone (PVP) (K 30, Sigma-Aldrich, USA), 1-methyl-2-pyrrolidinone (NMP) (99.5%, Sigma-Aldrich, USA) and N-N-Dimethylformamide (DMF) (99.8%, Sigma-Aldrich, USA) were used for PSf ultrafiltration substrates preparation. m-Phenylenediamine (MPD) flakes (99%, Aldrich, China) and 1,3,5-Benzenetricarbonyl chloride (TMC) (98%, Sigma-Aldrich, USA) dispersed in hexane (98%, Aldrich, China) were used for the IP process. Graphite (Sigma-Aldrich, USA), sodium nitrate (NaNO_3) (Beijing Chemical Factory, China), hydrogen peroxide (H_2O_2) (Beijing Chemical Factory, China), sulfuric acid (H_2SO_4) (Beijing Chemical Factory, China), and potassium permanganate (KMnO_4) (Sigma-Aldrich, USA) were used for GO nano-sheets preparation. For membranes chlorine resistance tests, sodium hypochlorite (NaClO) (Chemical Supply Pty Ltd, China) was used. Sodium chloride (NaCl) (ACS reagent, Beijing Chemical Factory, China) was dissolved in deionized water (DI) produced with a Milli-Q system (Millipore, USA) for FO tests.

Methods

Graphene oxide (GO) was synthesized from graphite powders by the classical Hummer's method (Hummers and Offeman, 1958; Hirata et al., 2004; Park and Ruoff, 2009). 1.0 g graphite and 0.5 g NaNO_3 were added into an Erlenmeyer flask with 23.0 ml concentrated H_2SO_4 solution, and then stirred under an ice bath. After that, 3.0 g KMnO_4 was added slowly for 2.0 h, then transferred the mixture into a 35.0°C water bath and continued to stir for 0.5 h. Then 46.0 ml DI water was slowly added, and the reaction was continued for 0.5 h as the temperature raised to 98.0°C. Finally, 140.0 mL DI water and 10.0 mL of H_2O_2 solution were added to the obtained solution to terminate the reaction. The mixture was filtered and then washed thrice with

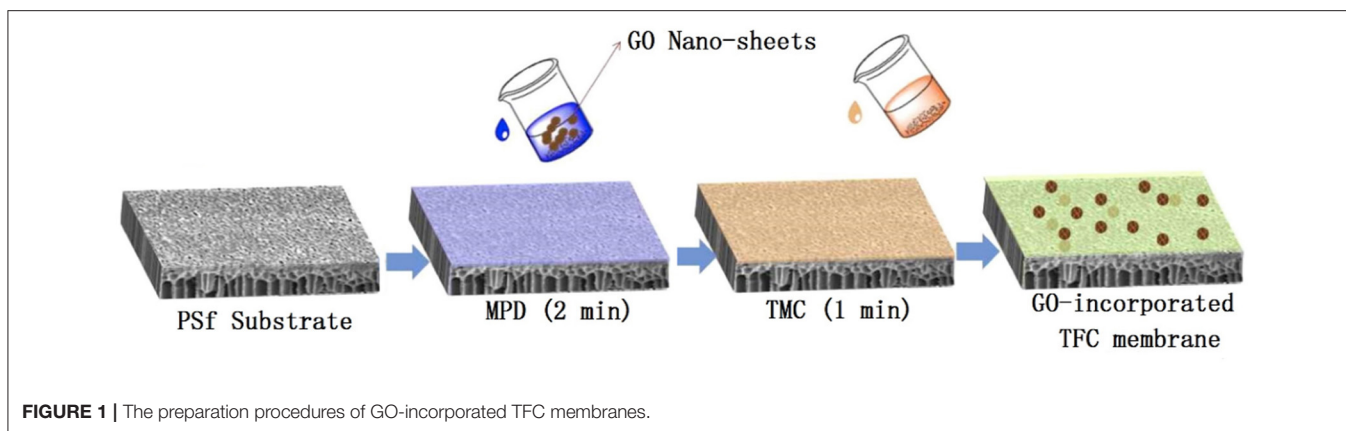


FIGURE 1 | The preparation procedures of GO-incorporated TFC membranes.

DI water to obtain the final product. Then, the as-prepared GO nano-sheets were washed three times with DI and methanol, respectively, to remove the unreacted chemical residuals. Finally, the obtained powders were freeze-dried for 48.0 h to obtain the GO nano-sheets.

Crystal structure of the synthesized GO nano-sheets was tested via a Miniflex 600 diffractometer (Rigaku, Japan) powder X-ray diffractometer (PXRD) in the 2θ range of $2\text{--}50^\circ$ at room temperature. Morphologies of the GO nano-sheets were taken with a field-emission scanning electron microscope (Merlin ZEISS GEMINI2) operating at 5 kV and 13 pA. Attenuated total reflection Fourier transform infrared (ATR-FTIR, Thermo Scientific Nicolet 6700) was used to characterize the GO nano-sheets. The XPS (VG Scientific, UK) measurements were also carried out for GO nano-sheets characterization using Mg $K\alpha$ radiation ($h\nu = 1,253.6\text{ eV}$). The C 1s spectra were recorded with the pass energy $E_p = 20\text{ eV}$ whereas the wide scans with $E_p = 100\text{ eV}$.

The Preparation of Polysulfone (PSf) Substrate

Flat-sheet PSf substrates were prepared by using a mixed PSf-PVP casting dope. 16.5 g PSf, 0.5 g PVP, 21.0 g NMP and 62.0 g DMF were magnetically stirred for at least 24.0 h and then left degassing for 8.0 h to prepare the casting dope. A thin layer ($100 \pm 10\ \mu\text{m}$) of the obtained dope was cast on a clean glass plate via a casting machine (Wu Han Zuoneng Instruments Ltd., China). The whole composite was exposed in the air for 10.0 s followed by immersing into a DI water bath to initiate phase inversion process. Once the substrate was peeled off from the glass plate, it was removed from the water bath, thoroughly rinsed with DI water for three times and then transferred to a 4°C DI water bath for storage till later use (Qin et al., 2013; Shen et al., 2015; Yu et al., 2019).

The Preparation and Characterization of Control and GO-Incorporated TFC Membrane

The synthesis procedure of the TFC-control membrane without GO was below (Wang et al., 2018a). The PSf substrate was first immersed in an aqueous solution containing 3.4 wt% MPD

TABLE 1 | Reagents for TFC series membranes preparation.

| Membranes | MPD (wt%) in aqueous phase | GO (wt%) in aqueous phase | MPD/GO solutions viscosity (cp) | TMC in organic phase (wt%) |
|-------------|----------------------------------|---------------------------------|--|----------------------------------|
| TFC-control | 3.4 | 0 | 60.00 | 0.15 |
| GO-1 | 3.4 | 0.0025 | 60.67 | 0.15 |
| GO-2 | 3.4 | 0.0050 | 60.67 | 0.15 |
| GO-3 | 3.4 | 0.0100 | 61.33 | 0.15 |
| GO-4 | 3.4 | 0.0150 | 62.00 | 0.15 |
| GO-5 | 3.4 | 0.0200 | 62.67 | 0.15 |

monomers for 2.0 min. Excess MPD solution was removed by a rubber roller. After that, the substrate was immersed into a 0.15 wt% TMC solution for 1.0 min to form the PA layer. The fabrication of GO-incorporated membranes was similar to that of TFC-control membrane, except that GO nano-sheets were added in the aqueous solution before IP process, as shown in **Figure 1** and **Table 1**. GO with various concentrations from 0.0025 to 0.02 wt% was dissolved in aqueous solution by ultra-sonication under an ice bath for 30.0 min. The GO/MPD-saturated substrates were immediately placed to react with the TMC/n-hexane solution for the formation PA layers. The synthesized GO-incorporated membranes were denoted by GO-1, GO-2, GO-3, GO-4, and GO-5, corresponding to a GO loading of 0.0025, 0.0050, 0.0100, 0.0150, and 0.0200 wt%, respectively. The as-prepared membranes were also rinsed with DI water thoroughly for three times and then stored in DI water at 4°C for later tests.

The morphologies of the TFC membranes surfaces and cross-sections (fractured in liquid nitrogen) were observed by FESEM (Merlin ZEISS GEMINI2). Fifteen random tests were conducted based on three different batch membranes in cross-sectional images for PA layer thickness tests. Water contact angles were measured using a contact angle system (Dataphysics OCA 20). For each membrane, ten measurements were performed for each of three independently prepared membranes. ATR-FTIR spectroscopy instrument (Thermo Scientific Nicolet

6700) was used to confirm the change of the PA layer functional groups.

Evaluation of TFC Membrane Desalination Performance

All the as-prepared membranes were tested in a lab-scale test system, which has been described in our previous work (Wang et al., 2018a,b). The co-current cross-flow velocity was 4.9 cm/s for both the feed and draw solutions. The temperatures of the feed and draw solutions were maintained at $20 \pm 0.5^\circ\text{C}$. 1.0 and 2.0 M NaCl solutions were used as the DSs and a balance (ML4002, METTLER TOLEDO) was connected to a computer to record weight changes of the permeated water at 30.0 s intervals. 10.0 mmol L⁻¹ NaCl solution were used as the feed solution (FS) and a conductivity meter was used to calculate the reverse solute flux of the membrane at 60.0 s intervals. Membranes were tested under two different modes: (1) active layer facing draw solution (AL-DS) mode; and (2) active layer facing feed solution (AL-FS) mode. Every test was conducted for 1.0 h in triplicate. The water permeation flux (J_w) (L • m⁻²h⁻¹, LMH), reverse solute flux (J_s) (g • m⁻²h⁻¹), and specific reverse solute flux (SRSF) (g • L⁻¹) were calculated by the same methods detailed in our previous work (Wang et al., 2018a,b).

Evaluation of Membrane and Chlorine Resistance

The chlorine resistance of the tested membranes was evaluated by exposing their top surfaces to a 1,000 ppm NaClO solution over different periods. The NaClO solutions were kept in dark and replaced every 2.0 h during the test to maintain a constant concentration. To access the as-prepared membranes chloride resistance quantitatively, a doubled increase value of SRSF was selected as an upper limit, indicating the PA layers were degraded dramatically by the active chlorine to be unacceptable in FO processes (Lu et al., 2017; Wang et al., 2018c). Before the membrane FO performance tests, these membranes were removed from NaClO solutions and then washed 3 times with DI water to avoid the residual chlorine oxidation during tests.

Determination of FO Membrane Transport and Structural Parameters

The transport and structural parameters of these as-prepared membranes, the water permeability coefficient (A), salt permeability coefficient (B), and structural parameter (S) were tested by a method developed by Elimelech's Group (Tiraferrri et al., 2013). The method includes a four-stage test, every stage using a DS with different concentration. The water permeation flux (J_w) and reverse solute flux (J_s) were measured through non-linear regression based on Equations (1) and (2), in every FO test stage. The presented data were the average values based on triplicated measurements.

$$J_w = A \left\{ \frac{\pi_D \exp\left(-\frac{J_w S}{D}\right) - \pi_F}{1 + \frac{B}{J_w} \left[1 - \exp\left(-\frac{J_w S}{D}\right)\right]} \right\} \quad (1)$$

$$J_s = B \left\{ \frac{C_D \exp\left(-\frac{J_w S}{D}\right) - C_F}{1 + \frac{B}{J_w} \left[1 - \exp\left(-\frac{J_w S}{D}\right)\right]} \right\} \quad (2)$$

where D is the bulk diffusion coefficient of the draw solute.

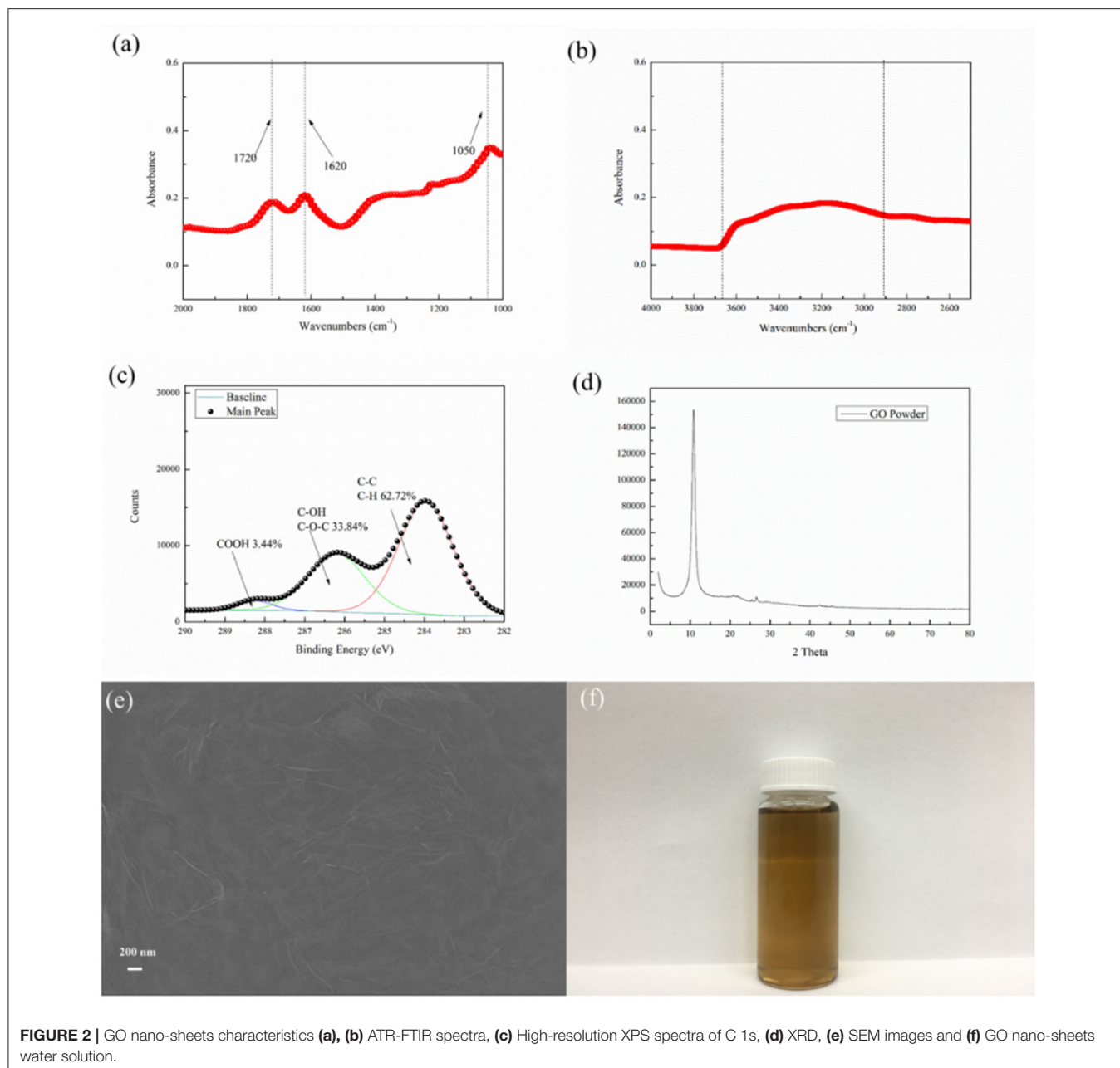
RESULTS AND DISCUSSIONS

GO Nano-Sheets Characteristics

The ATR-FTIR spectra for GO nano-sheets were presented **Figures 2a,b**. The presence of C–O bonds (1,050 cm⁻¹) in epoxy groups, C=C bonds (1,620 cm⁻¹) in unoxidized carbon crystal lattice, and C=O bonds (1,720 cm⁻¹) in carboxyl groups, can be observed in the synthesized GO nano-sheets, similar to Jiang's work (Jiang et al., 2014). Meanwhile, an intense band between 3,100 and 3,600 cm⁻¹ indicated that GO nano-sheets with many free hydroxyl groups can bridge hydrogen bonds and enhance intermolecular forces between GO nano-sheets and PA polymer chains. Moreover, the analysis of the chemical valence of elements can be used to estimate the oxidation degree of GO nano-sheets (Stankovich et al., 2007; Stoller et al., 2008; Zhou et al., 2010). The high-resolution XPS C 1s spectra of the GO were shown in **Figure 2c**, the peaks of 284.0, 286.2, and 288.3 eV can be attributed to C–C, C–H, C–O, and C=O groups, respectively. According to these peak areas, it is estimated that about 60% of C didn't undergo oxidation reaction, 33.84% of oxidized C contained C–O and 3.44% of oxidized C contained COOH. Moreover, the XRD pattern and SEM image of the GO nano-sheets were shown in **Figures 2d,e**, which are consistent with Leszek Stobinski et al.'s results (Stobinski et al., 2014). Finally, after the graphene oxidation, new oxygen-containing groups were formed on the surface, such as C=O, C–OH, C–O–C, etc., thus the aqueous GO solution (see **Figure 2f**) showed a typical light yellow color, which is similar to the reported characteristics in the literature (Masuda et al., 2002; Novoselov et al., 2004; Allen et al., 2009). Based on, the GO nano-sheets were successfully synthesized.

Membrane Characterization Membrane Morphology

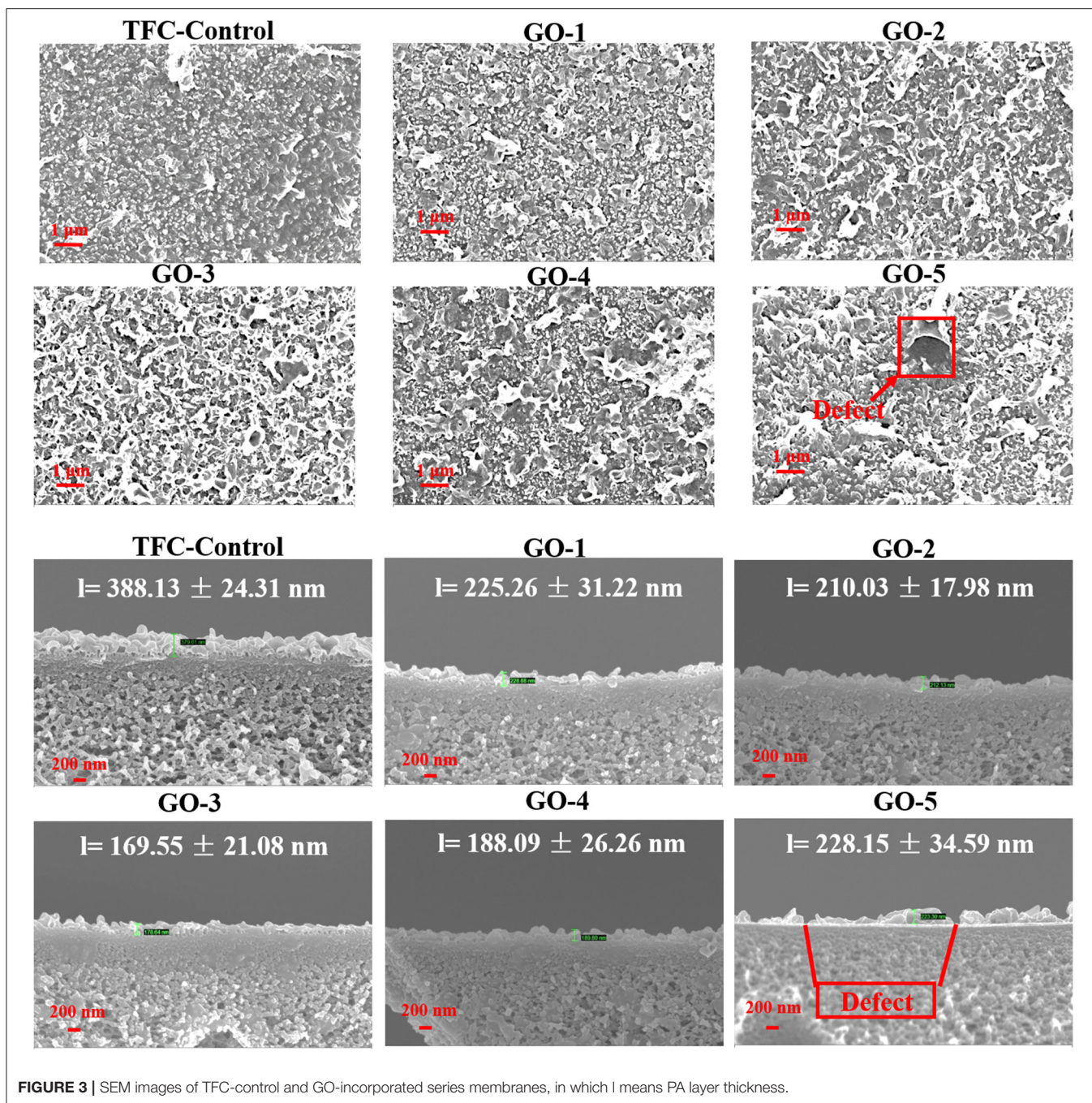
The surface and cross-section morphologies of the TFC-control and GO-incorporated series TFC membranes were investigated, as shown in **Figure 3**. All the membranes surfaces possessed "ridge and valley" or "flower" characteristics, which is the typical morphology of the PA membrane. Additional thin layers were observed on top PSf substrates via the cross-sectional SEM images, which confirms the successful reaction of interfacial polymerizations. Obviously, the incorporation of GO nano-sheets into the active PA layer can significantly affect the membrane surface as well as cross-sectional morphology. Compared to the pristine membrane, all the GO-incorporated membranes displayed denser and relatively smoother surfaces. Meanwhile, the PA layer thickness of the control TFC membrane was much higher than those of GO-incorporated TFC membranes. For example, GO-3 membrane had PA layer thickness of 169.55 nm, which is only about 1/2 of the control-TFC membrane. However, when the concentration of GO in



the aqueous phase increased to 0.0200 wt%, defects would be observed on the membrane surface as well as membrane cross section. At the same time, the PA layer thickness increased slightly compared to the control membrane, which might compromise membrane FO selectivity.

The remarkable changes of PA layers in GO-incorporated membranes may be contributed by the following reasons, as shown in **Figure 4**. Generally, TMC monomers are less soluble in the water phase, thus IP reaction happens in the organic phase. MPD monomers need to diffuse from the water phase to the organic phase to react with the TMC monomers (Luo et al., 2014). The substrate was saturated by the MPD/GO aqueous solution vertically, GO nano-sheets tend to position

along the membrane surface horizontally due to the Langmuir-Blodgett film deposition (Chae et al., 2015). The horizontal incorporation of GO nano-sheets would interfere the diffusion of MPD monomers, resulted in smoother active PA layers. In the meanwhile, hydrogen bonds presented in the hydroxyl groups of GO can contribute to a more compact chain structure. Moreover, these nano-sheets incorporation decreased the amount of MPD monomers and increased the viscosity of the aqueous solution (see **Table 1**), thus limited the reaction between MPD and TMC monomers and formed thinner active layers. However, when the loading in the aqueous phase increased to 0.0200 wt%, which caused the serve agglomerations of the GO nano-sheets, thus formed a defective interface enables MPD to further diffuse

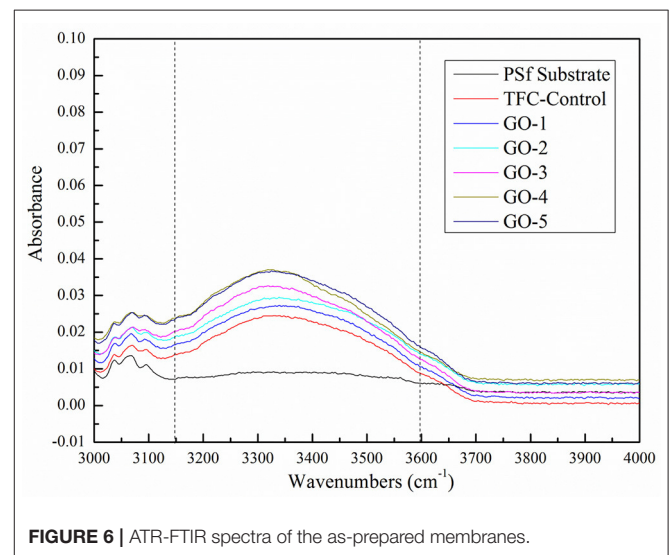
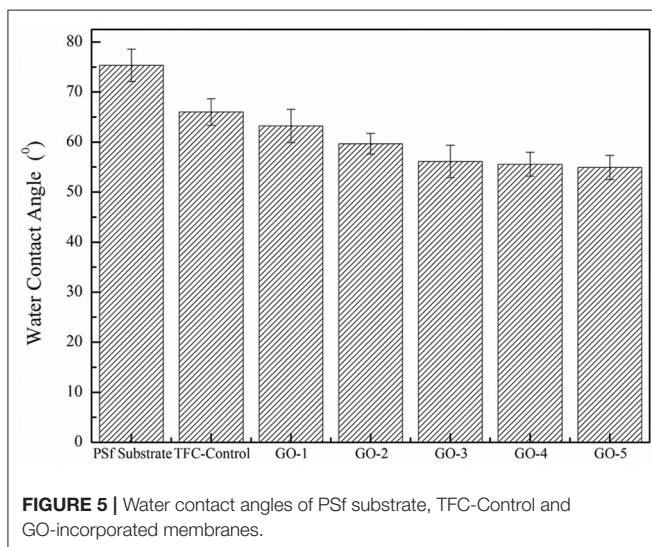
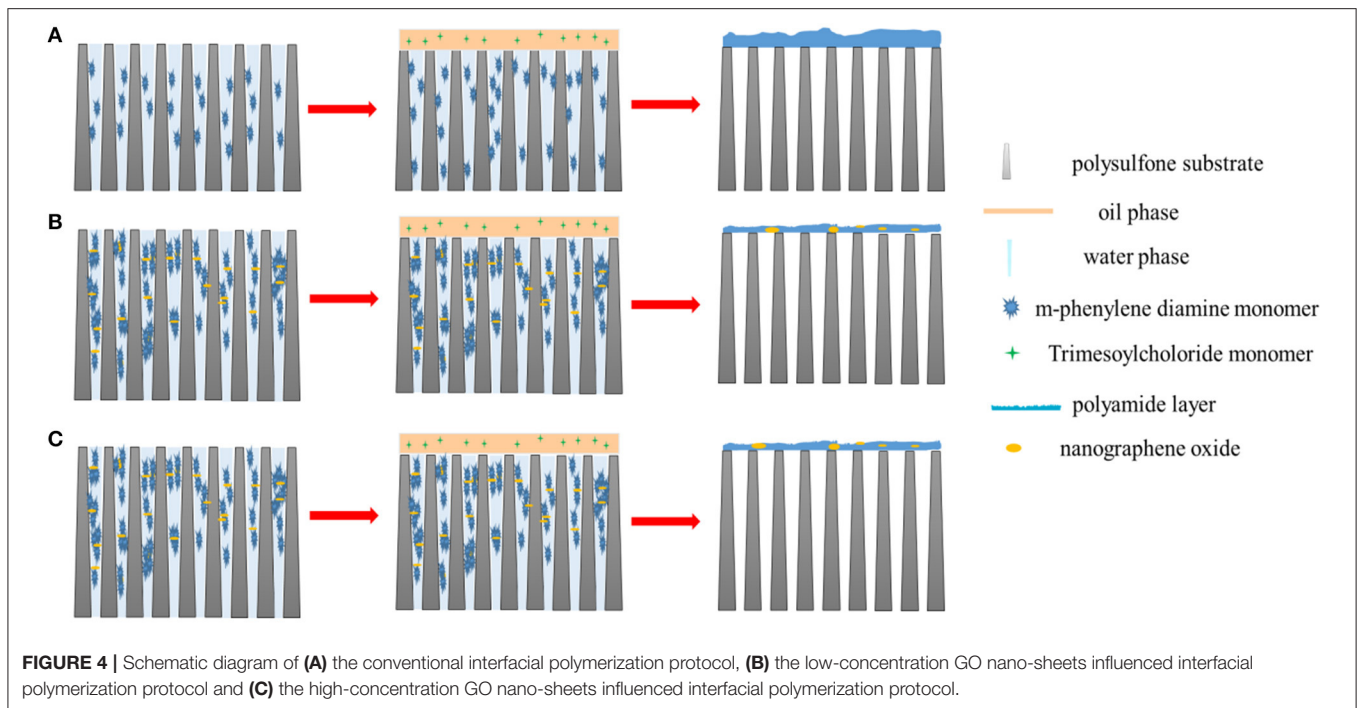


through the pristine PA layer, resulting in a slightly thicker PA layer.

Membrane Hydrophobicity

The GO nano-sheets with hydroxyl functional groups in the aqueous phase are expected to improve the membrane surface hydrophilicity, as shown in **Figure 5**. The water contact angle of the PSf substrate was relatively high at 75.3° , but after the GO incorporation, the water contact angles of all the GO-incorporated membranes were improved, indicating the successful incorporation of GO nano-sheets in

the PA layers. Moreover, the increase in the peak intensity of hydroxyl groups at about $3,100\text{--}3,600 \text{ cm}^{-1}$ was also found in all the GO-incorporated TFC membranes, as shown in **Figure 6**, which are attributed to O–H groups stretching vibration in GO nano-sheets, leading to more hydrophilic PA membrane surfaces (Stobinski et al., 2014). However, for the GO-4 and GO-5 membranes with high GO nano-sheets concentrations, the water contact angles only decreased from 56.1 to 54.9° , which indicates too high concentrations of GO showed slight influence on the membrane surface hydrophilicity. The GO-incorporated membranes had higher



hydrophilicity than the control sample might be related to the surface morphology and hydrophilic bulk of the membranes. Compared to the control membrane with a dense surface (see SEM image), the GO-incorporated membranes with a loose surface yielded a better wetting behavior likely due to the capillary effect. Apart from this, the GO-incorporated membranes had increased free volumes compared with the control membranes, which may be responsible for the improvement in the membrane wettability. Moreover, the GO-incorporated membranes with more O-H groups, leading to more hydrophilic PA membrane surfaces. As such, the GO-incorporated membranes had higher hydrophilicity than the control membrane.

Membrane Desalination Performance

Figure 7 shows the water fluxes of the FO membranes incorporated by different concentrations of GO nano-sheets in the AL-FS mode and the AL-DS mode with 1.0 and 2.0 M NaCl as draw solutions, respectively. It could be observed that the water fluxes of both AL-FS mode and AL-DS showed similar tendencies: with increasing concentrations of GO nano-sheets, the water fluxes initially went up and reached the optimal value typically being at 0.0100 wt%. Namely, the maximum water flux of GO-incorporated membrane was obtained when 0.0100 wt% of GO nano-sheets was added into the aqueous phase, with the water flux increasing 56.97% (from 7.32 to 11.49 L/m²h) in the AL-FS mode and 42.48% (from 10.17 to 14.49 L/m²h) in the AL-DS mode.

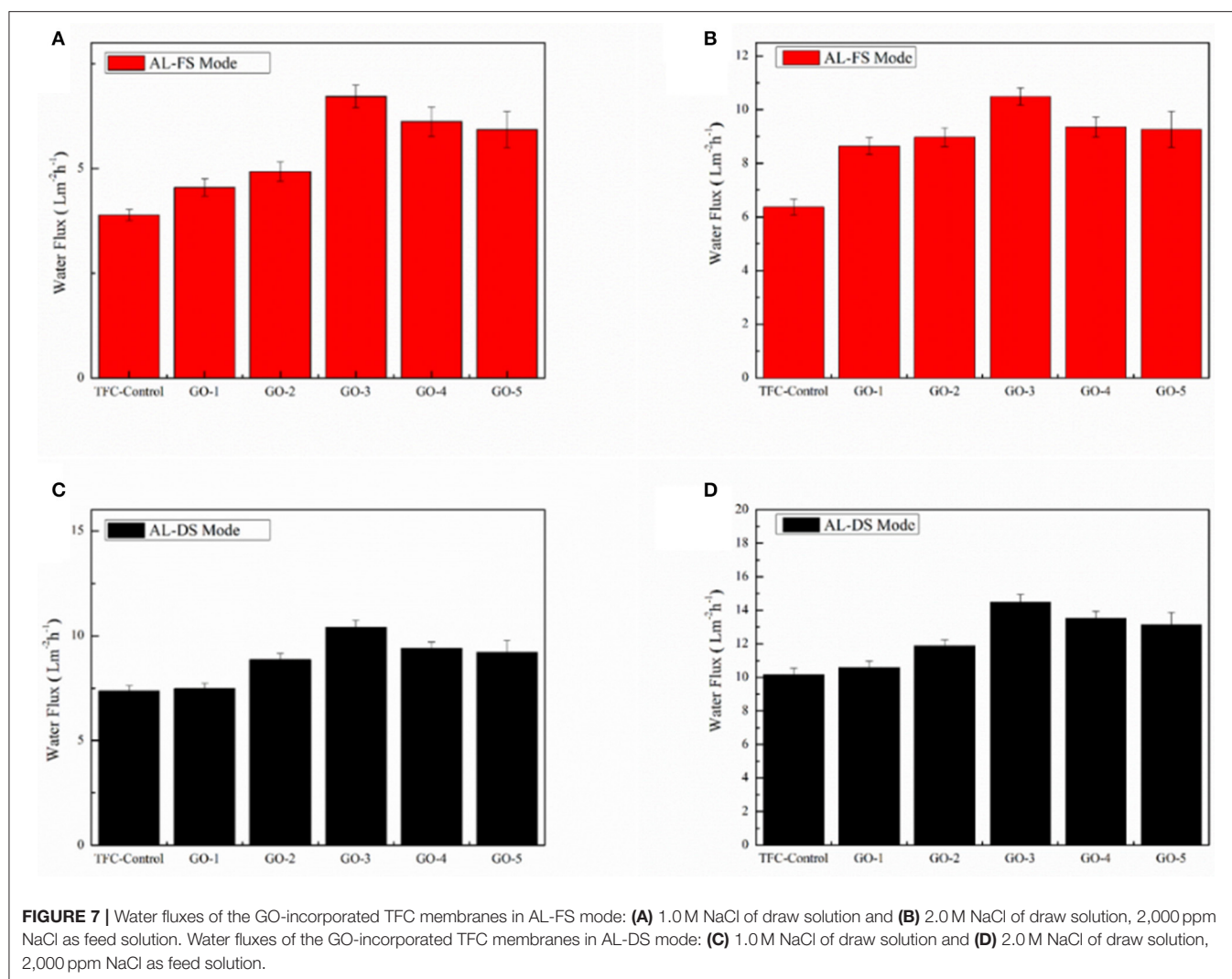


FIGURE 7 | Water fluxes of the GO-incorporated TFC membranes in AL-FS mode: **(A)** 1.0 M NaCl of draw solution and **(B)** 2.0 M NaCl of draw solution, 2,000 ppm NaCl as feed solution. Water fluxes of the GO-incorporated TFC membranes in AL-DS mode: **(C)** 1.0 M NaCl of draw solution and **(D)** 2.0 M NaCl of draw solution, 2,000 ppm NaCl as feed solution.

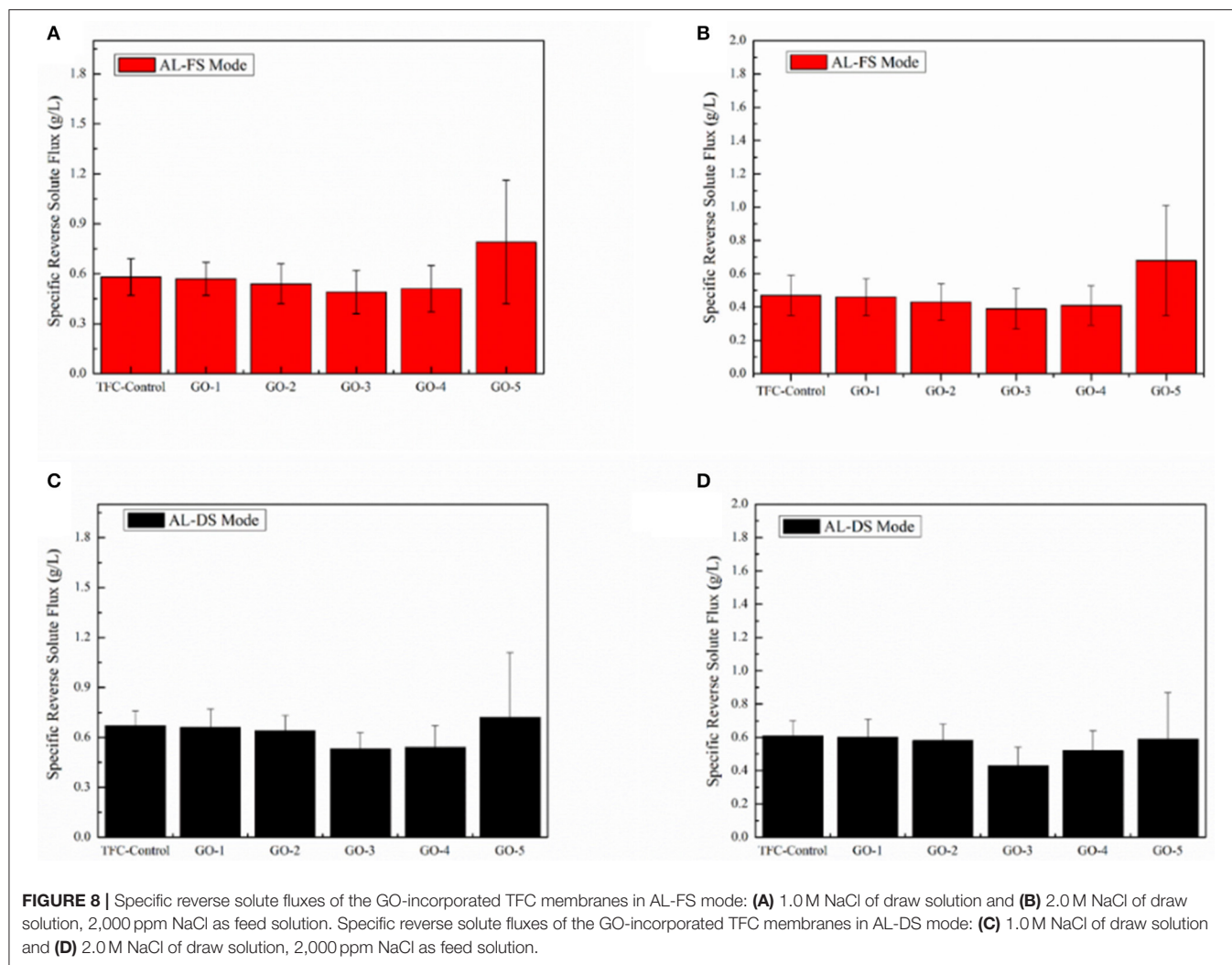
in the AL-DS mode when using 2.0 M NaCl solution as the draw solution. This may be due to the improvement of the hydrophilic properties of GO-incorporated membranes. The higher the hydrophilic properties of the membranes, the easier for the water molecules to pass through the membranes (He et al., 2015; Xia et al., 2015; Shi et al., 2018). In addition, the decrease of the thickness of active PA layer of GO-incorporated membrane will also lead to an increase in FO water flux. However, when the GO nano-sheets concentration was too high, the membrane water flux began to decrease, which might be ascribed to the slight increase in the thickness of the active layer.

Figure 8 shows the SRSFes of the FO membranes incorporated by different concentrations of GO nano-sheets in the AL-FS mode and the AL-DS mode with 1.0 and 2.0 M NaCl as draw solutions, respectively. The higher SRSF indicates relatively more solutes passing from the draw side to the feed side. Compared with the TFC-control membrane, the trend of SRSFes of the GO-incorporated membrane reduced and then increased along with increasing concentrations of GO nano-sheets. This is because the charge effect and two-dimensional

capillary effect of GO nano-sheets, the water molecules pass easily in the PA layer in the meanwhile reject effectively salt ions. Therefore, moderate incorporation of GO nano-sheets can effectively improve the FO membrane selectivity. However, excessive loading of GO nano-sheets would lead to a defective surface of the membrane, resulted in the dramatically increase of GO-5 membrane SRSF. In addition, comparing the selectivity of the membrane with 1.0 and 2.0 M NaCl as draw solution, it can be seen that the selectivity of the membrane with 2.0 M NaCl was slightly higher than that of the former. This may be due to the increase of osmotic pressure resulting in a denser active layer.

Membrane Separation and Transport Parameters

Table 2 studies the water permeability coefficient A , salt permeability coefficient B , and structural coefficient S value of GO-3 (the optimal membrane) and control membrane, respectively. The A value of control membrane was $0.206 \text{ LMHbar}^{-1}$, while this value of GO-3 increased significantly to $0.278 \text{ LMHbar}^{-1}$ when GO was introduced in aqueous



phase. This trend agrees well with the results of FO desalination performance tests. The improvement of water permeability should be ascribed to the enhancement of GO-3 membrane hydrophilicity. Compared with the water permeability coefficient, the salt permeability coefficient of GO-3 decreased sharply to 0.009 LMH, which may be attributed to the interception of salt ions by GO nano-sheets. The trend of B value also agreed well with the behavior of SRSF. As for the membrane structure parameter, GO-3 membrane displayed 452 μm , only 57.7% of the control membrane, this may be caused by the PA layer thickness decrease (Zhang et al., 2013). In addition, A/B ratio is an important parameter to evaluate FO membrane selectivity, and higher A/B ratio indicates higher selectivity. The A/B ratio of GO-3 membrane showed 67.1% higher than that of the TFC-control membrane, which confirmed again the high desalination performance of the GO-3 membrane.

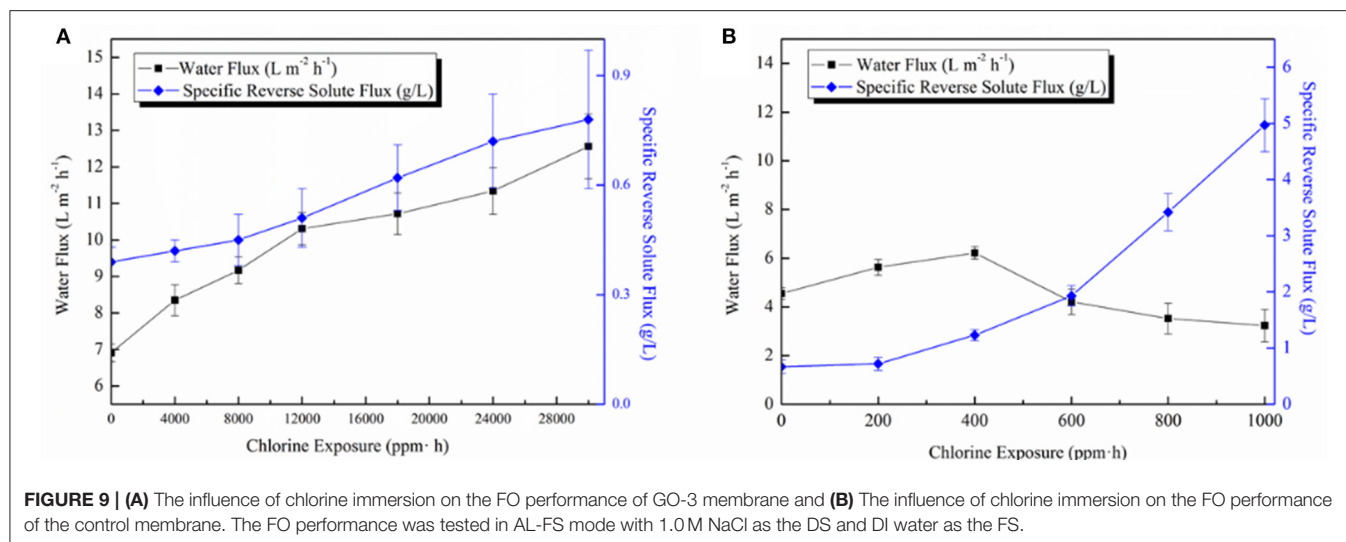
Membrane Chlorine Resistance

Membrane chlorine-resistance tests were conducted for both TFC-Control and GO-3 membranes as shown in **Figure 9**. For GO-3 membrane, a slow and mild increase of FO water flux as

TABLE 2 | Summary of the transport properties of the TFC-Control and GO-3 membrane.

| Names | A (LMHBar ⁻¹) | B-LMH | S (μm) | A/B (Bar ⁻¹) | R ² (J _w) | R ² (J _s) | CV (%) |
|-------------|---------------------------|-------|---------------------|--------------------------|----------------------------------|----------------------------------|--------|
| TFC-Control | 0.206 | 0.116 | 784 | 1.776 | 0.973 | 0.965 | 1.58 |
| GO-3 | 0.278 | 0.009 | 452 | 2.967 | 0.960 | 0.960 | 0.65 |

well as SRSF was observed during the chlorine-resistance test, which lasted up to as high as 30,000 ppm • h, before the SRSF value was doubled. The increased chlorine resistance of the GO-3 membrane might be attributed to hydrogen bonding between GO nano-sheets and PA layer blocking the replacement of amidic hydrogen with active chlorine. Moreover, the incorporated GO nano-sheets could keep the underlying PA chains from active chlorine attack. Therefore, a gradual increase of water flux due to the slow degradation of the PA layer was observed. At the same time, the surging rise of reverse solute flux was avoided because of the relatively compact and dense PA layer structure. As for the control membrane, the water flux increased initially but



eventually dropped to 70.9% of the original flux in 1,000 ppm • h, while the SRSF greatly increased from 0.67 to 4.97 g/L. The amide bonds of the raw PA layers are vulnerable to free chlorine and can be easily destroyed by the N-chlorination, Orton rearrangement, and direct ring chlorination reactions, leading to the PA layer free volume increase as well the polymer matrix flexibility. Thus, at the beginning of the degradation of PA layer, the water molecules can easily transfer the PA layer, however, because of the fast degradation of the PA layer, then, a sharp increase of SRSF was observed, which caused a RO-like concentration polarization on top of the active layer thus decreasing both membrane water permeability and selectivity. Apparently, the GO-3 exhibited a much slower PA layer destruction when exposed to free chlorine, thus possessed good chlorine resistance characteristics (75.0 times enhancement).

CONCLUSIONS

In this paper, a new type of TFC membranes was developed via using MPD/GO mixture as the aqueous phase for IP process. The GO nano-sheets were characterized by the FTIR, XRD, XPS, and SEM to confirm their successful syntheses. The GO-incorporated TFC membranes exhibited improved surface hydrophilicity and smoothness, as well as thin PA layer thickness, because of the affected diffusion rate of MPD monomers and increased aqueous phase solutions viscosity with the incorporation of GO nano-sheets. Compared with the control membrane, the desalination performance of the optimal membrane was significantly improved whereas only 0.0100 wt% GO nano-sheets was applied in this method. When 2.0M NaCl was used as the draw solution, the water

REFERENCES

Ali, M. E. A., Wang, L., Wang, X., and Feng, X. (2016). Thin film composite membranes embedded with graphene oxide for water desalination. *Desalination* 386, 67–76. doi: 10.1016/j.desal.2016.02.034

flux of GO-3 membrane increased 56.97% in AL-FS mode and 42.48% in AL-DS mode, at the same time, the SRSF of the membrane decreased indicated the selectivity of the membrane improved, which was due to the charge effect and two-dimensional capillary effect of GO nano-sheets made it easier for water molecules transfer and more effective for salt ions rejection. Therefore, the optimal GO-incorporated TFC membranes possessed higher water permeability, less salt permeability and lower structural parameter as compared to the control membrane. Moreover, the optimized membrane showed 75.0 times more chloride-resistant characteristics than the pristine membrane due to hydrogen bonding between GO nano-sheets and PA layer and the GO nano-sheets protection. The excellent water permeability and chloride resistance of this new type of membrane could facilitate wider applications of FO membranes in desalination applications.

DATA AVAILABILITY STATEMENT

All datasets generated for this study are included in the article.

AUTHOR CONTRIBUTIONS

All authors extensively discussed the results, reviewed the manuscript, and approved the final version of the manuscript to be published.

ACKNOWLEDGMENTS

YW acknowledges Mr. Min Liu from University of Melbourne for data analysis and collection.

Allen, M. J., Tung, V. C., Gomez, L., Xu, Z., Chen, L.-M., Nelson, K. S., et al. (2009). Soft transfer printing of chemically converted graphene. *Adv. Mater.* 21, 2098–2102. doi: 10.1002/adma.200803000

Chae, H.-R., Lee, J., Lee, C.-H., Kim, I.-C., and Park, P.-K. (2015). Graphene oxide-embedded thin-film composite reverse osmosis membrane with high

- flux, anti-biofouling, and chlorine resistance. *J. Memb. Sci.* 483, 128–135. doi: 10.1016/j.memsci.2015.02.045
- Darwish, M. A., and ElDessouky, H. (1996). The heat recovery thermal vapour-compression desalting system: a comparison with other thermal desalination processes. *Appl. Therm. Eng.* 16, 523–537. doi: 10.1016/1359-4311(95)00034-8
- Emadzadeh, D., Lau, W. J., and Ismail, A. F. (2013). Synthesis of thin film nanocomposite forward osmosis membrane with enhancement in water flux without sacrificing salt rejection. *Desalination* 330, 90–99. doi: 10.1016/j.desal.2013.10.003
- Emadzadeh, D., Lau, W. J., Matsuura, T., Hilal, N., and Ismail, A. F. (2014a). The potential of thin film nanocomposite membrane in reducing organic fouling in forward osmosis process. *Desalination* 348, 82–88. doi: 10.1016/j.desal.2014.06.008
- Emadzadeh, D., Lau, W. J., Matsuura, T., Ismail, A. F., and Rahbari-Sisakht, M. (2014b). Synthesis and characterization of thin film nanocomposite forward osmosis membrane with hydrophilic nanocomposite support to reduce internal concentration polarization. *J. Memb. Sci.* 449, 74–85. doi: 10.1016/j.memsci.2013.08.014
- Greenlee, L. F., Lawler, D. F., Freeman, B. D., Marrot, B., and Moulin, P. (2009). Reverse osmosis desalination: water sources, technology, and today's challenges. *Water Res.* 43, 2317–2348. doi: 10.1016/j.watres.2009.03.010
- Han, G., Zhang, S., Li, X., Widjojo, N., and Chung, T.-S. (2012). Thin film composite forward osmosis membranes based on polydopamine modified polysulfone substrates with enhancements in both water flux and salt rejection. *Chem. Eng. Sci.* 80, 219–231. doi: 10.1016/j.ces.2012.05.033
- Han, G., Zhao, B., Fu, F., Chung, T.-S., Weber, M., Staudt, C., et al. (2016). High performance thin-film composite membranes with mesh-reinforced hydrophilic sulfonated polyphenylenesulfone (sPPSU) substrates for osmotically driven processes. *J. Memb. Sci.* 502, 84–93. doi: 10.1016/j.memsci.2015.12.023
- He, L., Dumée, L. F., Feng, C., Velleman, L., Reis, R., She, F., et al. (2015). Promoted water transport across graphene oxide–poly(amide) thin film composite membranes and their antibacterial activity. *Desalination* 365, 126–135. doi: 10.1016/j.desal.2015.02.032
- Hirata, M., Gotou, T., Horiuchi, S., Fujiwara, M., and Ohba, M. (2004). Thin-film particles of graphite oxide 1. *Carbon* 42, 2929–2937. doi: 10.1016/j.carbon.2004.07.003
- Hu, M., and Mi, B. (2013). Enabling graphene oxide nanosheets as water separation membranes. *Environ. Sci. Technol.* 47, 3715–3723. doi: 10.1021/es400571g
- Hummers, W. S. Jr., and Offeman, R. E. (1958). Preparation of graphitic oxide. *J. Am. Chem. Soc.* 80:1339.
- Ionita, M., Vasile, E., Crica, L. E., Voicu, S. I., Pandeale, A. M., Dinescu, S., et al. (2015). Synthesis, characterization and *in vitro* studies of polysulfone/graphene oxide composite membranes. *Compos. B Eng.* 72, 108–115. doi: 10.1016/j.compositesb.2014.11.040
- Jiang, Z., Jiang, Z., Tian, X., and Chen, W. (2014). Amine-functionalized holey graphene as a highly active metal-free catalyst for the oxygen reduction reaction. *J. Mater. Chem. A* 2, 441–450. doi: 10.1039/c3ta13832a
- Khawaji, A. D., Kutubkhanah, I. K., and Wie, J.-M. (2008). Advances in seawater desalination technologies. *Desalination* 221, 47–69. doi: 10.1016/j.desal.2007.01.067
- Kong, F., Yang, H., Wang, X., and Xie, Y. F. (2014). Rejection of nine haloacetic acids and coupled reverse draw solute permeation in forward osmosis. *Desalination* 341, 1–9. doi: 10.1016/j.desal.2014.02.019
- Liu, Z., and Hu, Y. (2016). Sustainable antibiofouling properties of thin film composite forward osmosis membrane with rechargeable silver nanoparticles loading. *ACS Appl. Mater. Interfaces* 8, 21666–21673. doi: 10.1021/acsami.6b06727
- Lu, P., Liang, S., Zhou, T., Mei, X., Zhang, Y., Zhang, C., et al. (2016). Layered double hydroxide/graphene oxide hybrid incorporated polysulfone substrate for thin-film nanocomposite forward osmosis membranes. *RSC Adv.* 6, 56599–56609. doi: 10.1039/c6ra10080e
- Lu, P., Liang, S., Zhou, T., Xue, T., Mei, X., and Wang, Q. (2017). Layered double hydroxide nanoparticle modified forward osmosis membranes via polydopamine immobilization with significantly enhanced chlorine and fouling resistance. *Desalination* 421, 99–109. doi: 10.1016/j.desal.2017.04.030
- Lu, P., Liu, Y., Zhou, T., Wang, Q., and Li, Y. (2018). Recent advances in layered double hydroxides (LDHs) as two-dimensional membrane materials for gas and liquid separations. *J. Memb. Sci.* 567, 89–103. doi: 10.1016/j.memsci.2018.09.041
- Luo, H., Wang, Q., Zhang, T. C., Tao, T., Zhou, A., Chen, L., et al. (2014). A review on the recovery methods of draw solutes in forward osmosis. *J. Water Process Eng.* 4, 212–223. doi: 10.1016/j.jwpe.2014.10.006
- Ma, D., Peh, S. B., Han, G., and Chen, S. B. (2017). Thin-film nanocomposite (TFN) membranes incorporated with super-hydrophilic metal-organic framework (MOF) UiO-66: toward enhancement of water flux and salt rejection. *ACS Appl. Mater. Interfaces* 9, 7523–7534. doi: 10.1021/acsami.6b14223
- Marcovecchio, M. G., Mussati, S. F., Aguirre, P. A., Nicolás, J., and Scenna, (2005). Optimization of hybrid desalination processes including multi stage flash and reverse osmosis systems. *Desalination* 182, 111–122. doi: 10.1016/j.desal.2005.03.011
- Masuda, Y., Jinbo, Y., Yonezawa, T., and Koumoto, K. (2002). Templated site-selective deposition of titanium dioxide on self-assembled monolayers. *Chem. Mater.* 14, 1236–1241. doi: 10.1021/cm0107528
- Mazlan, N. M., Peshev, D., and Livingston, A. G. (2016). Energy consumption for desalination—a comparison of forward osmosis with reverse osmosis, and the potential for perfect membranes. *Desalination* 377, 138–151. doi: 10.1016/j.desal.2015.08.011
- Mi, B., and Elimelech, M. (2010). Organic fouling of forward osmosis membranes: fouling reversibility and cleaning without chemical reagents. *J. Memb. Sci.* 348, 337–345. doi: 10.1016/j.memsci.2009.11.021
- Niksefat, N., Jahanshahi, M., and Rahimpour, A. (2014). The effect of SiO₂ nanoparticles on morphology and performance of thin film composite membranes for forward osmosis application. *Desalination* 343, 140–146. doi: 10.1016/j.desal.2014.03.031
- Novoselov, K. S., Geim, A. K., Morozov, S. V., Jiang, D., Zhang, Y., Dubonos, S. V., et al. (2004). Electric field effect in atomically thin carbon films. *Science* 306, 666–669. doi: 10.1126/science.1102896
- Park, M. J., Phuntsho, S., He, T., Nisola, G. M., Tijing, L. D., Li, X.-M., et al. (2015). Graphene oxide incorporated polysulfone substrate for the fabrication of flat-sheet thin-film composite forward osmosis membranes. *J. Memb. Sci.* 493, 496–507. doi: 10.1016/j.memsci.2015.06.053
- Park, S., and Ruoff, R. S. (2009). Chemical methods for the production of graphenes. *Nat. Nanotechnol.* 4, 217–224. doi: 10.1038/nnano.2009.58
- Qin, Q., Hou, Z., Lu, X., Bian, X., Chen, L., Shen, L., et al. (2013). Microfiltration membranes prepared from poly(N-vinyl-2-pyrrolidone) grafted poly(vinylidene fluoride) synthesized by simultaneous irradiation. *J. Memb. Sci.* 427, 303–310. doi: 10.1016/j.memsci.2012.09.059
- Salehi, H., Rastgar, M., and Shakeri, A. (2017). Anti-fouling and high water permeable forward osmosis membrane fabricated via layer by layer assembly of chitosan/graphene oxide. *Appl. Surf. Sci.* 413, 99–108. doi: 10.1016/j.apsusc.2017.03.271
- She, Q., Wong, Y. K. W., Zhao, S., and Tang, C. Y. (2013). Organic fouling in pressure retarded osmosis: experiments, mechanisms and implications. *J. Memb. Sci.* 428, 181–189. doi: 10.1016/j.memsci.2012.10.045
- Shen, L., Li, L., Chen, J., Hong, H., Yu, H., Hou, Z., et al. (2015). Effects of molecular weight distribution (M_w) on the performances of the polyethersulfone (PES) ultrafiltration membranes. *J. Memb. Sci.* 490, 220–226. doi: 10.1016/j.memsci.2015.04.068
- Shi, M., Wang, Z., Zhao, S., Wang, J., Zhang, P., and Cao, X. (2018). A novel pathway for high performance RO membrane: preparing active layer with decreased thickness and enhanced compactness by incorporating tannic acid into the support. *J. Memb. Sci.* 555, 157–168. doi: 10.1016/j.memsci.2018.03.025
- Stankovich, S., Dikin, D. A., Piner, R. D., Kohlhaas, K. A., Kleinhammes, A., Jia, Y., et al. (2007). Synthesis of graphene-based nanosheets via chemical reduction of exfoliated graphite oxide. *Carbon* 45, 1558–1565. doi: 10.1016/j.carbon.2007.02.034
- Stobinski, L., Lesiak, B., Malolepszy, A., Mazurkiewicz, M., Mierzwa, B., Zemek, J., et al. (2014). Graphene oxide and reduced graphene oxide studied by the XRD, TEM and electron spectroscopy methods. *J. Electron Spectros. Relat. Phenomena* 195, 145–154. doi: 10.1016/j.elspec.2014.07.003
- Stoller, M. D., Park, S., Zhu, Y., An, J. H., and Ruoff, R. S. (2008). Graphene-based ultracapacitors. *Nano Lett.* 8, 3498–3502. doi: 10.1021/nl802558y

- Sukitpaneent, P., and Chung, T. S. (2012). High performance thin-film composite forward osmosis hollow fiber membranes with macrovoid-free and highly porous structure for sustainable water production. *Environ. Sci. Technol.* 46, 7358–7365. doi: 10.1021/es301559z
- Tiraferrì, A., Yip, N. Y., Straub, A. P., Castrillon, S. R.-V., and Elimelech, M. (2013). A method for the simultaneous determination of transport and structural parameters of forward osmosis membranes. *J. Memb. Sci.* 444, 523–538. doi: 10.1016/j.memsci.2013.05.023
- Verbeke, R., Gómez, V., and Vankelecom, I. F. J. (2017). Chlorine-resistance of reverse osmosis (RO) polyamide membranes. *Prog. Polym. Sci.* 72, 1–15. doi: 10.1016/j.progpolymsci.2017.05.003
- Wang, Y., Fang, Z., Xie, C., Zhao, S., Ng, D., and Xie, Z. (2018c). Dopamine incorporated forward osmosis membranes with high structural stability and chlorine resistance. *Processes* 6, 1–12. doi: 10.3390/pr6090151
- Wang, Y., Fang, Z., Zhao, S., Ng, D., Zhang, J., and Xie, Z. (2018a). Dopamine incorporating forward osmosis membranes with enhanced selectivity and antifouling properties. *RSC Adv.* 8, 22469–22481. doi: 10.1039/c8ra03166e
- Wang, Y., Li, X., Cheng, C., He, Y., Pan, J., and Xu, T. (2016). Second interfacial polymerization on polyamide surface using aliphatic diamine with improved performance of TFC FO membranes. *J. Memb. Sci.* 498, 30–38. doi: 10.1016/j.memsci.2015.09.067
- Wang, Y., Li, X., Zhao, S., Fang, Z., Ng, D., Xie, C., et al. (2018b). Thin-film composite membrane with interlayer decorated metal-organic framework UiO-66 toward enhanced forward osmosis performance. *Ind. Eng. Chem. Res.* 58, 195–206. doi: 10.1021/acs.iecr.8b04968
- Xia, S., Yao, L., Zhao, Y., Li, N., and Zheng, Y. (2015). Preparation of graphene oxide modified polyamide thin film composite membranes with improved hydrophilicity for natural organic matter removal. *Chem. Eng. J.* 280, 720–727. doi: 10.1016/j.cej.2015.06.063
- Xue, W., Yamamoto, K., and Tobino, T. (2016). Membrane fouling and long-term performance of seawater-driven forward osmosis for enrichment of nutrients in treated municipal wastewater. *J. Memb. Sci.* 499, 555–562. doi: 10.1016/j.memsci.2015.11.009
- Yu, W., Liu, Y., Xu, Y., Li, R., Chen, J., Liao, B.-Q., et al. (2019). A conductive PVDF-Ni membrane with superior rejection, permeance and antifouling ability via electric assisted *in-situ* aeration for dye separation. *J. Memb. Sci.* 581, 401–412. doi: 10.1016/j.memsci.2019.03.083
- Zhang, S., Fu, F., and Chung, T.-S. (2013). Substrate modifications and alcohol treatment on thin film composite membranes for osmotic power. *Chem. Eng. Sci.* 87, 40–50. doi: 10.1016/j.ces.2012.09.014
- Zhao, S., Zou, L., Tang, C. Y., and Mulcahy, D. (2012). Recent developments in forward osmosis: opportunities and challenges. *J. Memb. Sci.* 396, 1–21. doi: 10.1016/j.memsci.2011.12.023
- Zhou, Y., Bao, Q., Varghese, B., Tang, L. A., Tan, C. K., Sow, C. H., et al. (2010). Microstructuring of graphene oxide nanosheets using direct laser writing. *Adv. Mater.* 22, 67–71. doi: 10.1002/adma.200901942

Conflict of Interest: The authors declare that the research was conducted in the absence of any commercial or financial relationships that could be construed as a potential conflict of interest.

Copyright © 2020 Li, Wang, Han, Wang, Han, Liu, Zhou, Shang and Xie. This is an open-access article distributed under the terms of the Creative Commons Attribution License (CC BY). The use, distribution or reproduction in other forums is permitted, provided the original author(s) and the copyright owner(s) are credited and that the original publication in this journal is cited, in accordance with accepted academic practice. No use, distribution or reproduction is permitted which does not comply with these terms.